Journal of Catalysis 318 (2014) 170–178

Contents lists available at ScienceDirect

Journal of Catalysis

journal homepage: www.elsevier.com/locate/jcat

Effect of Ag, pH, and time on the preparation of Ag-functionalized zinc oxide nanoagglomerates as photocatalysts

Alma Berenice Jasso-Salcedo [a], Gabriela Palestino [b], Vladimir A. Escobar-Barrios [a,*]

[a] Instituto Potosino de Investigación Científica y Tecnológica (IPICYT), División de Ciencias Ambientales, Camino a la Presa San José 2055, Lomas 4a sección, C.P. 78216, San Luis Potosí, Mexico
[b] Universidad Autónoma de San Luis Potosí (UASLP), Facultad de Ciencias Químicas, Av. Manuel Nava No.6, Zona Universitaria, C.P. 78210, San Luis Potosí, Mexico

ARTICLE INFO

Article history:
Received 19 February 2014
Revised 2 June 2014
Accepted 5 June 2014

Keywords:
Functionalization
Ag/ZnO photocatalysts
Surface response methodology
Photocatalytic activity
Bisphenol-A

ABSTRACT

Photodeposition and impregnation methods for the functionalization of zinc oxide nanoagglomerates with silver nanoparticles were studied. The effect of reaction conditions such as nominal amount of stabilized silver nanoparticles, pH, and time on functionalization efficiency was investigated. The functionalized zinc oxide was characterized by X-ray diffraction, electron microscopy, N_2 physisorption, infrared spectroscopy, and UV–vis spectroscopy. The results showed that UV irradiation promoted the homogeneous dispersion of strongly bonded silver nanoparticles on ZnO. In addition, hydroxyl surface content and absorption in the visible region of the spectra suggest improvement of photocatalytic activity. The ZnO functionalized with silver by photodeposition and impregnation methods showed four and two times higher reaction rates, respectively, for bisphenol-A degradation compared with pure ZnO. Hence, the proposed functionalization methods represent a useful approach to synthesizing photocatalysts with the potential to be used in degradation of endocrine-disrupting compounds.

1. Introduction

Zinc oxide (ZnO) is a photocatalyst with adequate efficiency for photodegradation of dissolved contaminants in aqueous solutions [1,2]. It also has biomedical and antibacterial applications [3,4] and has been used for sensing and piezoelectric devices due to semiconductor properties such as direct band gap and high (60 meV) excitation binding energy [5,6]. The characteristic band gap of each material is related to the ease of charge transfer between the valence band and the conduction band, giving a photocatalytic capacity to the semiconductor. The goal of engineered semiconductors is to achieve a narrow band gap in order to be photoactivated with lower-energy radiation such as visible light. The band gap energy of ZnO and titanium dioxide (TiO_2), the latter a well-known and extensively used photocatalyst, is basically the same (3.2 eV). However, the valence and conduction bands exhibit differences in electric potential, whose reported values are in the range of −0.45 to 2.75 eV vs. NHE and −0.1 to 3.1 eV vs. NHE for ZnO and TiO_2, respectively [7,8]. This gives advantages to ZnO for catalyzing specific reduction reactions at lower potentials. Other important advantages of ZnO are photonic efficiency, chemical stability, null human cell toxicity [9], and low cost. Moreover, the optical and electronic properties of ZnO photocatalysts might be improved by controlling their surface area, particle size and shape, and polar/nonpolar surface orientation [10,11]. For all these reasons, nanometric ZnO can become a photocatalytic material with renewed applications for degradation of low concentrations of endocrine disruptors, pharmaceutical compounds and other emergent contaminants dissolved in aqueous solutions. In addition, the surface modification of ZnO with nanosized Ag has received attention, since it increases the half-life of both the charge carriers [12] (excited electrons and holes, e^*–h^+) in the ZnO surface after light absorption and the secondary active species generated (free radicals, i.e., ·OH). The metallic bond of Ag acts as a sink for photoexcited electrons, which reduce the recombination of the charge carriers in ZnO and increase the path length of the electrons and their sensitivity to visible light [12,13]. Despite their importance, there are some subjects that need consideration: (i) deposition yield of Ag, since it is usually low (<100%), (ii) distribution of Ag, which is not always homogeneous, and (iii) reaction condition optimization.

Recent developments in green synthesis of Ag nanoparticles using microorganisms [14] or harmless reducing agents [15] have led to homogeneous size and specifically shaped nanoparticles with catalytic properties. Those findings open up the possibility of new Ag nanoparticle sources to be used as surface modifiers of photocatalytic materials such as ZnO. Also, the use of stabilized

* Corresponding author. Fax: +52 444 8342010.
E-mail address: vladimir.escobar@ipicyt.edu.mx (V.A. Escobar-Barrios).

http://dx.doi.org/10.1016/j.jcat.2014.06.008
0021-9517/

Ag nanoparticles in the functionalization of photocatalysts makes feasible the use of green, simple, and low-cost methodologies without sacrificing size, shape, and properties in general.

In this paper, we describe the functionalization of ZnO nanoagglomerates with Ag nanoparticles (Ag/ZnO). Our strategy includes the use of water-dispersible Ag nanoparticles (AgNPs) for functionalization of ZnO in aqueous media through photodeposition (PD) and impregnation (IMP) methodologies. We demonstrate that photodeposition and impregnation methods can achieve homogeneous dispersion of AgNPs on ZnO surface.

Several authors report low AgNPs doping yields, usually not higher than 50% [16,17]. Therefore, we propose to use the actual amount of AgNPs attached to ZnO surface as a measured of the functionalization efficiency (FE) as a criterion to optimize the reaction conditions, namely pH, time, and nominal amount of AgNPs, for functionalization of ZnO.

2. Experimental section

2.1. Preparation of Ag/ZnO photocatalyst

Zinc oxide nanoagglomerates (VP AdNano ZnO 20 DW, Degussa Co., Essen, Germany) and AgNPs water stabilized by an anionic surfactant (CITD-Peñoles, Torreon, Mexico) were used as received without further purification. AgNPs solution is a noncommercial sample, which was characterized as having a concentration of 8×10^{-2} mol/L and particle size of 7 nm. We must point out that composition of the anionic surfactant is an industrial secret; however, basic characterization was done in order to define the catalytic mechanisms during preparation of the photocatalysts. The Ag/ZnO photocatalysts were obtained by photodeposition and impregnation methods as follows: for both methods, a suspension containing ZnO and AgNPs was adjusted at a desired initial pH using 0.1 N HCl and/or 0.5 N NaOH; the pH values for testing were below and above the point of zero charge (PZC) of ZnO nanoagglomerates (PZC = 9.3). For the photodeposition method (PD), the suspension (10 g/L ZnO) was irradiated using UV (λ_{max} = 254 nm, 3.4 mW/cm^2) during determined reaction time under magnetic stirring. For the impregnation method (IMP), the suspension (25 g/L ZnO) was only mechanically mixed during determined reaction time under room conditions. In order to remove non-attached AgNPs from the ZnO surface, the sample was submitted to centrifugation/redispersion cycles in distilled water and ethanol solutions several times. The photodeposited samples were dried at 80 °C for 8 h. The impregnated samples were calcined at 300 °C for 1 h. Finally, all the samples were stored in the dark. The nomenclature of the samples is as follows: *x*Ag/ZnO-PD*yz* and *x*Ag/ZnO-IMP*yz*, where *x* means the nominal amount of AgNPs (*x* = 0.1–5% w/w), *y* means the initial pH (*y* = 7–11), and *z* means the reaction time (*z* = 0.5–5 h).

2.2. Experimental design

An experimental design and a response surface methodology (RSM) were used to gain a better understanding of the effect of three parameters on the functionalization of ZnO with AgNPs. RSM is a useful tool for studying several variables with a reduced number of experiments usually described by the quadratic model. RSM has been applied successfully to the optimization of reaction conditions in degradation of organic compounds [18]. In the present study, the central composite design (CCD) and data analysis were established using MINITAB 14. The dependent variable, also known as the response, was the actual amount of AgNPs attached to the ZnO surface as a measure of the functionalization efficiency, which was defined by the following Eq. (1):

$$\mathrm{FE} = \frac{\text{actual amount Ag}}{\text{nominal amount Ag}} \times 100 \tag{1}$$

The amount of AgNPs was defined as Eq. (2):

$$\mathrm{Ag}\ \%\ \mathrm{w/w} = \frac{\text{weight Ag}}{\text{weight Ag} + \text{weight Zn}} \times 100 \tag{2}$$

The independent variables were the following: nominal amount of AgNPs, pH, and time, as shown in Table 1. The experimental range was based on published reports [19,20]. After running a total of 20 experiments, including 5 replicates at the center point, a second-order (quadratic) model was used to fit the experimental data that express the functionalization efficiency as a function of independent variables, Eq. (3)

$$Y = b_0 + b_1x + b_2y + b_3z + b_{11}x^2 + b_{22}y^2 + b_{33}z^2 + b_{12}xy + b_{13}xz + b_{23}yz \tag{3}$$

where Y is the response, b_0 the constant coefficient, and b_1 to b_{23} the linear, quadratic, and second-order coefficients of *x*, *y* and *z* independent variables. The model fit quality was expressed by R^2 and R^2_{adj}, while the model coefficients were evaluated by *P*-value ($P < 0.05$). The experimental and predicted actual amount of AgNPs for each experimental condition are shown in Table A.1 (see the Online Appendix).

2.3. Characterization of Ag/ZnO photocatalyst

The quantitative determination of silver and zinc content in the samples was carried out by inductively coupled plasma optical emission spectroscopy (ICP-OES) using a 730-ES spectrometer from Varian Inc. The silver quantification and distribution were obtained through energy energy-dispersive X-ray analysis (EDX) using a FIB Dual Beam FEI Helios 600 HRSEM microscope. The Brunauer–Emmet–Teller (BET) surface area was obtained by using N_2 sorption at −196 °C (ASAP 2020, Micromeritics). The presence or absence of surfactant after functionalization was observed by Fourier transform infrared spectrometry (FTIR, Nicolet 6700, Thermo Scientific). The effect of adding silver nanoparticles onto the crystal phases of ZnO was evaluated by X-ray diffraction with Cu Kα radiation (XRD, BRUKER D8, Advance). The morphology of Ag/ZnO was analyzed using an FEI Tecnai G2 F30 S-Twin TEM microscope. The optical properties were observed by solid-state UV–vis spectroscopy (Varian Cary 4000 UV–Vis, Agilent Technologies) from 300–600 nm.

2.4. Photocatalytic activity

The photocatalytic activities of the samples were evaluated following the bisphenol-A degradation. An aqueous suspension of bisphenol-A (>99%, Sigma Aldrich, Mexico) (50 mL, 10 ppm) and 0.05 g of photocatalyst were placed in a glass container. Prior to irradiation, the solution was mechanically mixed for 30 min in darkness. The solution was irradiated by 302 nm light using a UV lamp (3UVTM lamp, UVP, CA, USA) placed at 8 cm from the top of the solution. The experiments were carried out at pH = 10.5, 20 ± 1 °C without an external oxygen supply. Samples were collected at regular time intervals and centrifuged to remove the photocatalyst. The concentration of bisphenol-A was determined by high performance liquid chromatography (HPLC, Mod. 1200 SERIES, Agilent Technologies), using acetonitrile and water as the mobile phase. The reaction rate of bisphenol-A degradation was obtained assuming a pseudo-first-order reaction model using the following equation, Eq. (4):

$$-\ln(C/C_0) = K_{app}\, t \tag{4}$$

where K_{app} is the apparent rate constant, and *C* and C_0 the concentrations of bisphenol-A at certain irradiation times *t*. K_{app} was

Table 1
Experimental values and coded levels of independent variables.

Variables	Coded	Photodeposition			Impregnation		
Nominal amount AgNPs (% w/w)	*x*	0.1	0.3	1	0.1	1	5
pH	*y*	7	9	11	7	9	11
Time (h)	*z*	0.5	0.75	1	1	2	5

obtained from the slope of the $-\ln(C/C_0)$ vs. time plot. The normalization of K_{app} as a function of the active area was obtained using the BET surface area of the photocatalyst. The TiO_2 (Degussa "Aeroxide" P25, BET surface area $50 \pm 15 m^2/g$) was used as a photocatalyst reference.

3. Results and discussion

3.1. Mechanism of ZnO functionalization with AgNPs

It is well known that surfactants containing anionic functional groups promotes the dispersion of nanoparticles, keeping their particle size intact [21–24]. However, experimental conditions such pH and concentration of nanoparticles have a great strong influence on dispersion stability. In this work, we used AgNPs dispersed in anionic surfactant for the functionalization of ZnO and the mechanisms for both functionalization methods were proposed.

Scheme 1A describes the mechanism of functionalization of ZnO by photodeposition method. The mechanism considers stabilized AgNPs addition using the photogenerated electron–hole pairs and free radicals on ZnO surface as follows. After the ZnO and AgNPs are placed together, the electrical double layer is shortened as repulsion forces disappear at pH close to the point of zero charge. Under UV light irradiation, the electron–hole pair diffuses to the ZnO surface to produce free radicals (·OH, $^{-}$·O). Both primary and secondary reactive species promote the decomposition of the surfactant, leading to the AgNPs deposition. In addition, the formation of ionic silver (Ag^+) also takes place on the ZnO surface due to the direct oxidation of AgNPs (Ag^+/Ag^0, +0.799 eV vs. NHE) by holes (+2.75 eV vs. NHE). The insertion of ionic silver into the crystalline structure of ZnO can occur at the same time as they are reduced again to zerovalent form (Ag^0) by photoexcited electrons. Such insertion of Ag^+ could promote strong interaction between AgNPs and ZnO surface that enhances electron transport, reducing recombination and improving the photocatalytic activity. The by-products of surfactant decomposition and their possible accumulation decrease the pH values from 11 to 8 (Table A.2 of the Online Appendix). Nonattached AgNPs were washed out at the end of the functionalization process.

Scheme 1B describes the functionalization of ZnO by the impregnation method. As mentioned before, the electrical double layer between AgNPs and ZnO was reduced since nonionized surfactant was present at under alkaline conditions, meaning that electrical repulsion was absent. The surfactant acts as a coupling agent and the strong interactions prevents AgNPs wash off from the ZnO surface. A high concentration of AgNPs in water solution tends to form clusters, as a way to minimize the surface energy, while nonattached clusters are easily washed away. In the impregnation method, the surfactant solution was decomposed during the heating step (at 300 °C) in order to release AgNPs onto the ZnO surface.

3.2. Experimental design

The photocatalytic activity of Ag-doped ZnO has recently been studied [25,26], attributing this property was attributed to the size of the nanoparticles [27] and the synthesis method [28], therefore making the comparison between author results more challenging. However, it should be taken into account that differences in the photocatalytic activity are related to the uncertain metal content of the photocatalyst reported. It is well known that doping yields are lower than 100% [16,17,25], and even some authors do not even measure it. In this work, we decided to determine the actual amount number of AgNPs attached to the ZnO surface in order to assess structure–performance associations and photocatalytic performance comparisons.

The effect of synthesis parameters on the actual amount of AgNPs attached to the ZnO surface during the functionalization process was studied through RSM, allowing the experimental data to be fit into a quadratic model as well as the optimized conditions to maximize the response. The analysis of variance (ANOVA) confirms that the model was statistically significant ($P < 0.05$) for both functionalization methods (Table A.3 in the Online Appendix). The coefficients of the model terms, *P*-value, R^2, and R^2_{adj}, after exclusion of the insignificant terms, are shown in Table 2.

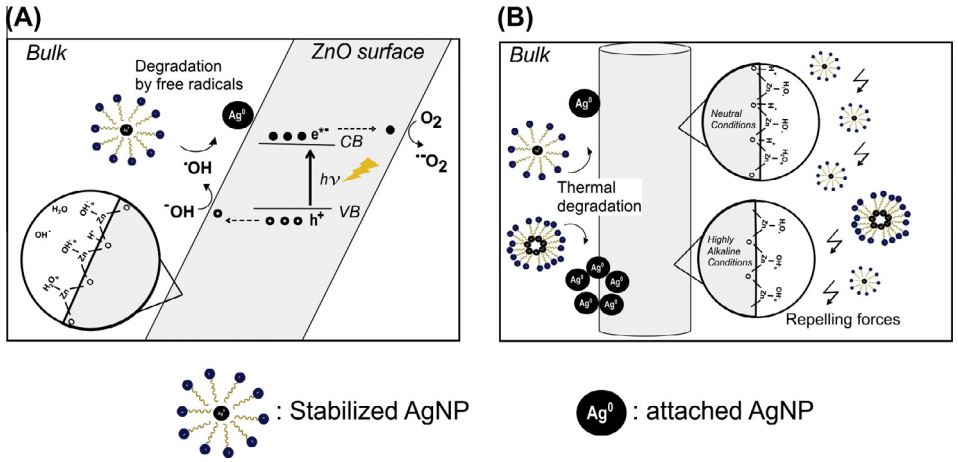

Scheme 1. The mechanism of functionalization of ZnO with AgNPs by photodeposition method (A) and impregnation method (B).

Table 2
Estimated regression coefficients and *P*-values of the quadratic model.

Coded term	Coefficient		*P*-value	
	Photodeposition (R^2 = 0.985, R^2_{adj} = 0.977)	Impregnation (R^2 = 0.902, R^2_{adj} = 0.856)	Photodeposition	Impregnation
Constant	0.574	1.719	<0.0001**	<0.0001**
x	0.508	0.202	<0.0001**	0.003*
y	0.008	−0.112	0.674	0.062
z	0.013	0.049	0.510	0.387
x^2	0.066	−1.315	0.198	<0.0001**
y^2	−0.101	−0.207	0.017*	0.068
z^2	−0.057	0.088	0.146	0.550
xy	0.041		0.075	NS

NS: not statistically significant.
* $P < 0.05$ significant.
** $P < 0.001$ highly significant.

The R^2 value shows that the model explain 98.5% and 90.2% of the experimental data of the ZnO functionalization by photodeposition and impregnation methods, respectively. We must to point out that functionalization efficiency higher than 100% has not physical sense and it could imply that all the added silver nanoparticles were attached to ZnO surface. The probable reasons for a functionalization efficiency value higher than 100% could be attributed to the following facts: a nonlinear concentration response of the technique in such this concentration range, a low accuracy of the equipment, or experimental error in the added silver solution. All those these reasons, together or individually, could contribute to an overestimation of the functionalization efficiency. The visualization of the interactive effect of the two most significant synthesis parameters was possible through 3D response surface plots shown in Fig. 1.

Fig. 1A shows the actual amount of AgNPs on ZnO photocatalyst, obtained by the photodeposition method, as a function of the nominal amount of AgNPs and pH at fixed time. From the plot, the response increases with increasing nominal amount of AgNPs. This could be due to diffusion problems of AgNPs from the bulk of the solution to the ZnO surface in such low quantities (i.e., 0.1% w/w). On the other hand, the response increases slightly when pH is close to the point of zero charge of ZnO (PZC = 9.3). This can be attributed to the neutralization of the ZnO surface charge that allows the interaction with the nonionized surfactant, as the repulsion forces are absent. Regarding the optimization, a nonunique optimized response can be obtained because of the experimental range studied in this work gets to a rising ridge-type response surface; however, a desired value of AgNPs on the ZnO surface could be predicted from the model.

Fig. 1B shows the 3D surface plot for the impregnation method. The actual amount of AgNPs deposited on ZnO increases with the increase of the nominal amount of AgNPs, reaching a maximum (∼3% w/w), and then the response decreases. This could be explained by the destabilization of the repelling forces between individual AgNPs at such high concentrations (>3% w/w) ending in the formation of agglomerates or clusters. Since nanoparticles minimize their surface energy by forming agglomerates [29], they do not attach to the ZnO surface. Unattached silver agglomerates are washed out of the ZnO surface, giving low functionalization efficiency. Low loading efficiencies for the impregnation method were also reported by Zanella et al. [16]. However, the experimental range evaluated made possible to attain optimal reaction conditions to maximize the functionalization efficiency. The proposed optimal conditions are pH = 9, reaction time 300 min, and nominal amount of 2.8% w/w of AgNPs.

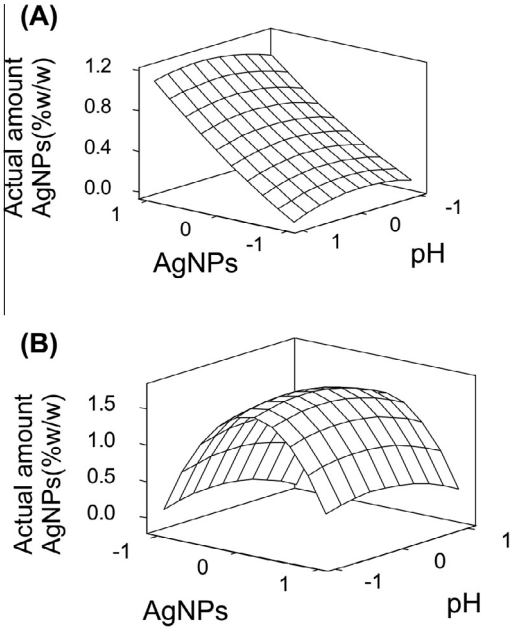

Fig. 1. 3D surface plot of actual amount of AgNPs for photodeposition method (A) and impregnation method (B).

3.3. Physicochemical characterization

Fig. 2A shows the X-ray diffraction patterns of Ag/ZnO obtained by photodeposition and impregnation. The diffraction pattern of ZnO shows peaks attributed to crystalline planes (100), (002), (101), (102), (110), (103), (112), and (201) corresponding to hexagonal wurtzite of zinc oxide (Card JCPDS 36-1451). The diffraction pattern of the stabilized AgNPs solution exhibits the planes (111), (200), and (220), which matches to the face-centered-cubic (fcc) crystal structure of silver (Card JCPDS 04-0783). In the diffraction patterns of Ag/ZnO photocatalyst, we observed the major plane (111) of metallic Ag, which confirms its presence on the ZnO surface, even when 1% w/w AgNPs was added.

Fig. 2A shows that impregnation samples keep the characteristic peaks of ZnO unchanged. Regarding the photodeposited samples, Fig. 2B shows a slight peak shift toward low angles and decreased peak intensity for samples with 1% w/w AgNPs, while no change was detected at 0.1% w/w AgNPs. Chu and co-workers reported the alteration of ZnO microtubules due to acidic pH, which causes a reduction of peaks intensity [30]. In our paper, we attributed the changes of ZnO crystalline structure to the insertion of silver nanoparticles because of UV irradiation exposure. The calculated lattice parameters of pure ZnO (a = 3.2275 Å, c = 5.1735 Å) and Ag/ZnO-PD11,1 photocatalyst (a = 3.2413 Å, c = 5.1896 Å) using XRD data shows an increase of the lattice

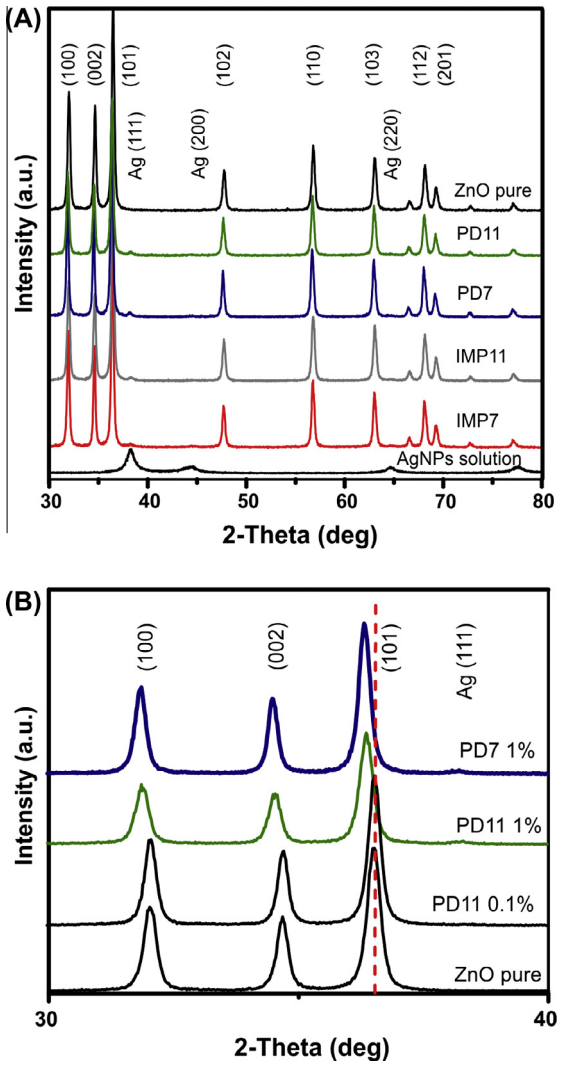

Fig. 2. XRD patterns of 1% w/w Ag/ZnO obtained by photodeposition and impregnation methods (A). Zoom in the XRD spectra of Ag/ZnO obtained by photodeposition (B).

parameters as expected. It has been reported that insertions of metallic ions into Zn sites promotes the expansion of the lattice parameters due to different ionic radii [31]. In our study, the UV irradiation could promote interstitial insertion of Ag^{+} (ionic radius = 0.122 nm) on ZnO (ionic radius of Zn^{2+} = 0.072 nm) as follows: the photogenerated holes in the valence band lead to partial oxidation of AgNPs, producing ionic silver (Ag^{+}), and subsequent insertion on the ZnO crystalline structure. From the obtained results, we confirmed that the functionalization of ZnO by the photodeposition method promotes a strong interaction between AgNPs and the ZnO surface.

It is challenging to control the particle size of metallic nanoparticles because it is the nanoparticles' nature to form agglomerates [29]. Thus, to find out whether AgNPs' size was maintained after ZnO functionalization, the average particle size of AgNPs was estimated by the Scherrer formula [32] as a first approximation. Table 3 shows the silver crystallite size of Ag/ZnO photocatalyst samples, which is at least twice (15–26 nm) that calculated for the stabilized AgNPs (7.11 nm). This result could indicate partial agglomeration of silver nanoparticles on ZnO surface.

Fig. 3 shows TEM images of stabilized AgNPs and 1% w/w Ag/ZnO photocatalyst. Fig. 3A shows stabilized AgNPs of spherical shape and defined boundaries. The histogram of the silver crystallite sizes shows AgNPs of 7.8 nm average size 7.8 nm (Fig. 3B), which is in agreement with the average crystallite size found by XRD analysis (7.11 nm; see Table 3). Fig. 3C and D shows the heterogeneous morphologies of ZnO (sphere, tetrapod, rod, and other irregular forms). The arrows point toward both AgNPs and AgNPs agglomerates on the ZnO surface, which is in agreement with the XRD suggestions. The high-magnification TEM image of Ag/ZnO-PD11, 1 sample (Fig. 3E) shows AgNPs of high crystallinity and homogeneously distributed on ZnO surface. The well-defined lattice fringes and continuity confirm the strong interaction between AgNPs and ZnO. The histogram on Fig. 3F shows the Ag nanoparticle size distribution on both photodeposited and impregnated samples. The results indicate the functionalization of ZnO with single-anchored AgNPs of particle size smaller than the particle size on stabilized AgNPs of the precursor solution. This could be explained by the formation of new metal seeds via direct Ag oxidation by holes or via indirect Ag oxidation by free radicals of more positive potential than the Ag^{+}/Ag^{0} pair (Ag^{+}/Ag^{0}, +0.799 eV vs. NHE). The differences in particle size between both used methods, TEM and XRD, are explained in terms of the fundamentals of the analytic technique (detection limits and sensitivity). Transmission electronic microscopy lend to detects single nanoparticles smaller than 1 nm in a punctual analysis that become representative of the sample if the number of nanoparticles analyzed (n) is large, while X-ray diffraction is a bulk analysis limited by the silver content in the sample and the assumption of regular particle shape for the Scherrer formula. Furthermore, Sakthivel et al. [33], among other authors, claim smaller size of metal nanoparticles when no peak appears in the XRD spectra of metal-doped TiO_2 due to the lack of sensitivity of the analysis. In our study, we describe the presence of the peak corresponding to silver nanoparticles even when the nominal silver content is 1% w/w. However, the calculations of the Scherrer formula were influenced for the nanoparticle size population of 15 nm up to 25 nm particle size. This means that XRD analysis does not discriminate between small and large nanoparticles. This does not reflect a conflict for with the existence of nanoparticles of smaller size as shown in TEM images (Fig. 3E and F).

In order to support TEM observations of homogeneous distribution of AgNPs (see Fig. 3C), two methods of silver quantification were used. The first one was silver quantification in solution by ICP-OES (bulk quantification) and the second was by EDX elemental analysis coupled to TEM (surface and punctual quantification). The results in Table 3 shows the congruence between the two quantitative analyses and confirms that the two functionalization methods did not show differences in promoting homogeneous distribution of AgNPs over ZnO.

To our knowledge, only a few authors have reported the uniform deposition of metallic nanoparticles over ZnO and CeO_2 starting from pre-formed nanoparticles by high-power techniques [23,24,34], but our study is the first to show the bulk modification of ZnO with stabilized AgNPs and achieve its homogeneous distribution at under ambient conditions.

The porosity profile of the samples was determined by N_2 isotherm adsorption–desorption. A Type II isotherm with an H3-type hysteresis loop was observed for pure ZnO and functionalized ZnO, which correspond to a microstructure containing macropores [35] or micrometric cavities around ZnO NPs (Fig. A.1 in the Online Appendix). The pore diameter of Ag/ZnO samples decreased to half in comparison with pure ZnO (Table 3). This could be explained by two possibilities: (i) macropore obstruction and (ii) formation of agglomerates. As we discussed before, the initial amount of AgNPs and pH are key parameters to induce the agglomeration of both AgNPs and ZnO. Table 3 shows that BET surface area decreases in all the Ag/ZnO photocatalysts (~17 m^2/g); however, it was considerably larger than that reported for pure ZnO (7–12 m^2/g) and comparable to that of doped ZnO/Ag (10–23 m^2/g) previously reported [35,36]. BET surface area has been related to the active

Table 3
Physicochemical properties of Ag/ZnO photocatalysts.

Sample	Ag (% w/w) by ICP-OES	Ag (% w/w) by EDX	Average Ag crystallite size (nm)[a]	Average pore diameter (nm)	BET surface area (m^2/g)	ZnO surface area coated (%)[b]
ZnO	–	–	–	216.63	22.04	–
AgNPs	–	–	7.11	–	–	–
1%PD7,1	1.093	0.78	25.76	100.56	17.58	0.36
1%PD11,1	1.147	1.55	19.34	126.58	16.20	0.54
1%IMP7,2	1.203	1.39	21.97	117.23	17.45	0.46
1%IMP11,2	0.366	1.10	15.25	93.13	16.59	0.21

[a] The average corresponds to experimental values obtained by the Scherrer formula [32] from the (1 1 1) plane from XRD.
[b] Calculations of the ZnO surface area coated by AgNPs taking into account data from columns 2, 4, and 6; see calculations in Online Appendix A.

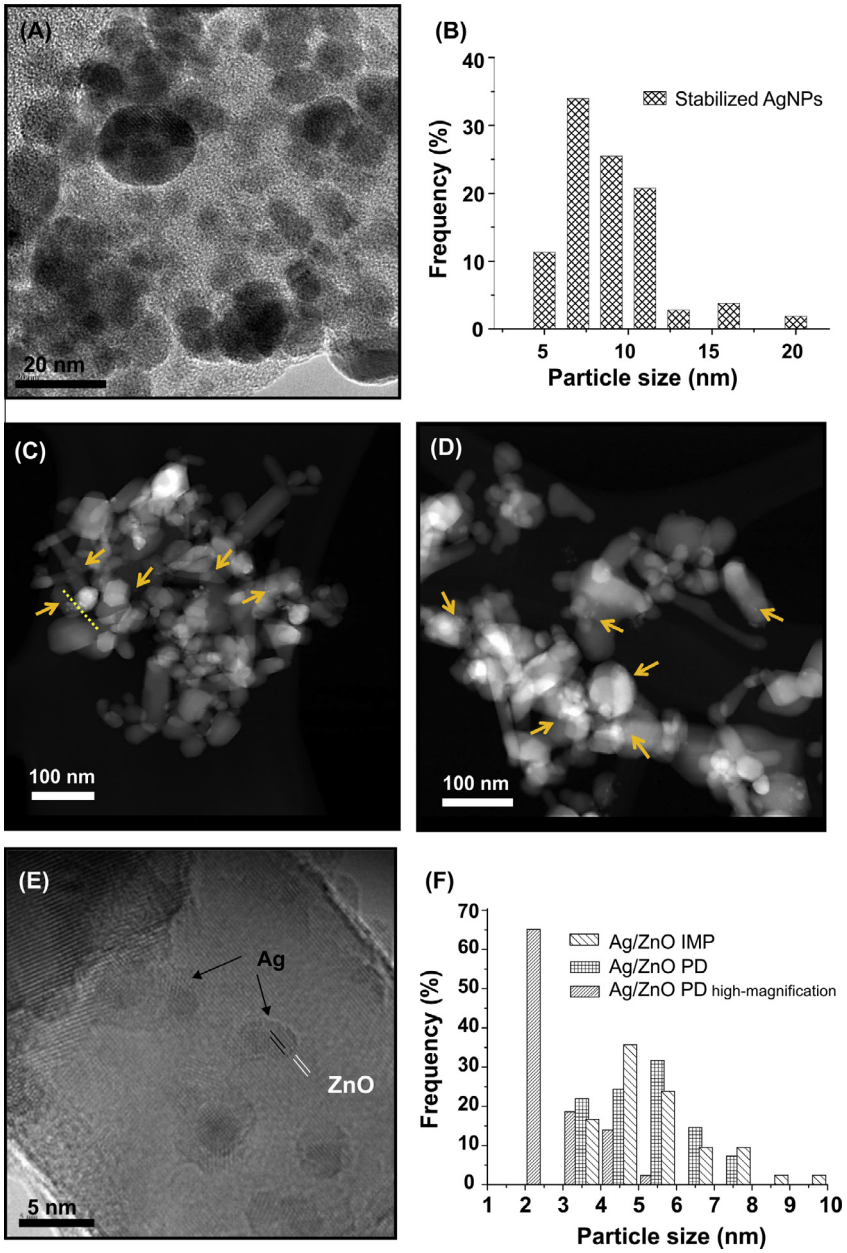

Fig. 3. TEM images of stabilized AgNPs (A and B) and 1% w/w Ag/ZnO photocatalyst prepared by the photodeposition (C and E: high-magnification) and impregnation (D) methods. Frequency histogram of AgNPs size before (B, $n = 106$) and after (F, $n = 40$ each one) ZnO functionalization.

surface area for the photocatalysis; however, other aspects must be considered, i.e., morphology and surface defects [27,28,37,38], crystalline orientation, and ionic strength [30]. Therefore, the decrease of BET surface area in our study surely is not a disadvantage, since the photocatalytic performance was improved as shown below.

We must point out the need for balance between AgNP size and the coated ZnO active area as a key parameter for the highest photocatalytic activity. In order to know the nominal ZnO active area coated by 1% w/w Ag, we consider the AgNPs average diameter of AgNPs in the original solution, the nominal amount of AgNPs (1% w/w = 0.00008 mol Ag), and the ZnO BET surface area (22 m^2/g). The calculations showed that 1.62% of the ZnO surface area would be coated by 7-nm AgNPs. (Calculations are detailed in the Online Appendix.) The calculations for Ag/ZnO samples show less surface covered by AgNPs (Table 3) because silver crystallite size from XRD analysis was considered. These calculations show that a small portion of the ZnO surface area was covered with AgNPs for the electron trapping process and reduce the recombination rate.

Fig. 4 shows the FTIR spectra of pure ZnO, AgNPs solution, and Ag/ZnO. In the FTIR spectrum of the AgNPs solution, the peaks at 3305 and 1637 cm^{-1} can be assigned to the O—H and C=O functional groups, respectively. The weak peaks at 2827 cm^{-1} correspond to C—H bonds from the —CH_2 of the body of the surfactant (Fig. 2.A in the Online Appendix). The characteristic peak of S—H around 2500 cm^{-1} assigned to the thiol group [21] was not detected because it was already bound to the Ag nanoparticle surface. However, the S atom of the thiol group was detected by EDX analysis on pure AgNPs (Fig. 2.A). These results indicated that the anionic surfactant contained exposed carboxylic acid groups that maintained water dispersion of the Ag nanoparticles.

In the spectra of Ag/ZnO, the broad peak at 3400 cm^{-1} corresponds to the O—H, which could be due either to (i) water, because of the humidity of the samples, or (ii) the surface hydroxyl content caused by the functionalization process. The peak at 2650 cm^{-1} can be assigned to the S—H bond due to the accumulation of thiol groups on the ZnO surface. In support of the latter proposal, it should be noted that the bands at 1390 and 1256 cm^{-1} correspond to the C—H group of —CH_2, owing to the residual molecules of the surfactant solution remaining after functionalization processes. This suggests that the functionalization methods proposed induce the functionalization of ZnO and Ag surfaces with hydroxyl (—OH), S—H, and C—H groups. Several authors report that the surface hydroxyl content could be increased if the surface termination of ZnO crystals allowed it, i.e., Zn-terminated polar surface ZnO (0001)-Zn and nonpolar ZnO (10−10) [11,38]. The more surface hydroxyl content there is on the ZnO surface, the more hydroxyl radicals there are for the oxidation reaction and higher photocatalytic activity might have the photocatalyst.

In addition to the surface properties, the interaction with light defines the photocatalytic performance; for this reason, the absorption of light needs to be considered. Fig. 5 shows the UV–vis spectra of the samples with two peaks: 360 and 435–460 nm. The first peak, at 360 nm, was the absorbance corresponding to ZnO due to the optical transition of electrons from valence to conduction band. The band gap (E_g) values were estimated using the wavelength (nm) of the intersection between the slope of the curve and the Y axis in the following equation Eq. (5):

$$E_{g=1240/\lambda} \quad (5)$$

The band gap for pure ZnO photocatalyst was estimated as 3.20 eV and was increased after silver addition (3.24 eV).

The second peak, at 435–460 nm, corresponds to the surface plasmon (SP) resonance of AgNPs. Fig. 5 shows a shift of the broader SP peak toward the visible region of the spectrum in comparison from the peak of the stabilized AgNPs solution (410 nm, data not shown). The position and width of SP have been related to the size, content, and environment of the AgNPs [26,39]. In our study, this shift and narrow SP peak at 435 nm can be explained by the strong interaction between Ag and ZnO in photodeposited samples. Despite the different Ag–ZnO interaction in the functionalized samples, the effect of surface-localized plasmon resonance of silver remains to improve both the spectral selectivity in the visible region and the photocatalytic activity.

3.4. Photocatalytic activity

The effect of the functionalization method on the photocatalytic activity of the photocatalysts synthesized was studied in the bisphenol-A degradation. Fig. 6A shows the normalized concentration vs. irradiation time for selected functionalized photocatalysts and the photocatalyst reference. The results indicate that after functionalization of ZnO nanoagglomerates with Ag nanoparticles, the samples enhanced its photoactivity compared with pure ZnO. Fig. 6A shows that the maximum photocatalytic degradation efficiency corresponding to 1% w/w Ag/ZnO-PD11,1 photocatalyst was 86% after 120 min of irradiation time under UV light. Even when the mineralization of bisphenol-A was not accomplished, the degradation efficiency was comparable to those reported in the literature using ZnO [40,41].

The active surface area for photocatalysis has been related to the BET surface area; hence, the reaction rate needs to be normalized. Fig. 6B shows the apparent rate constant normalized for sur-

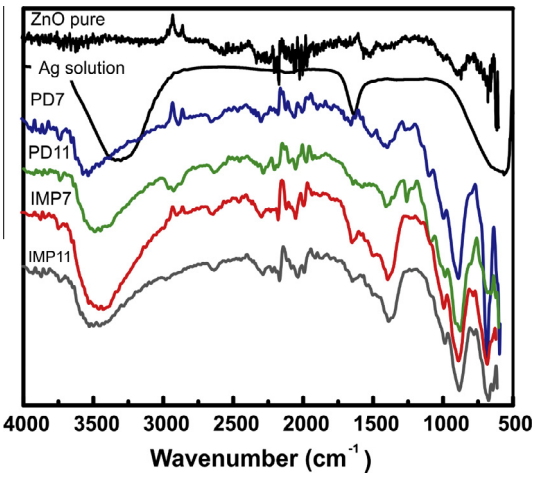

Fig. 4. FTIR spectra of 1% w/w Ag/ZnO.

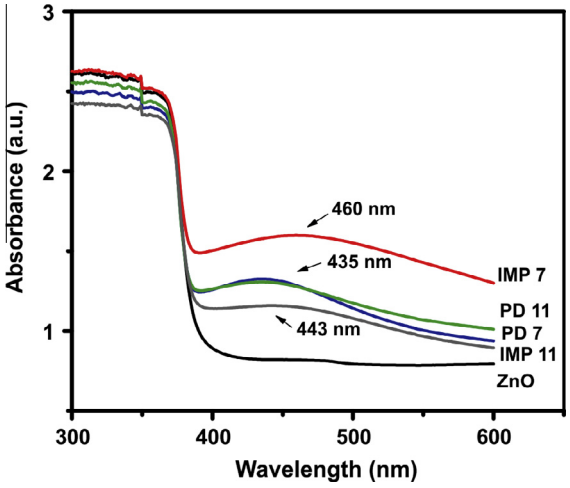

Fig. 5. UV–vis spectra of 1% w/w Ag/ZnO prepared by photodeposition and impregnation methods.

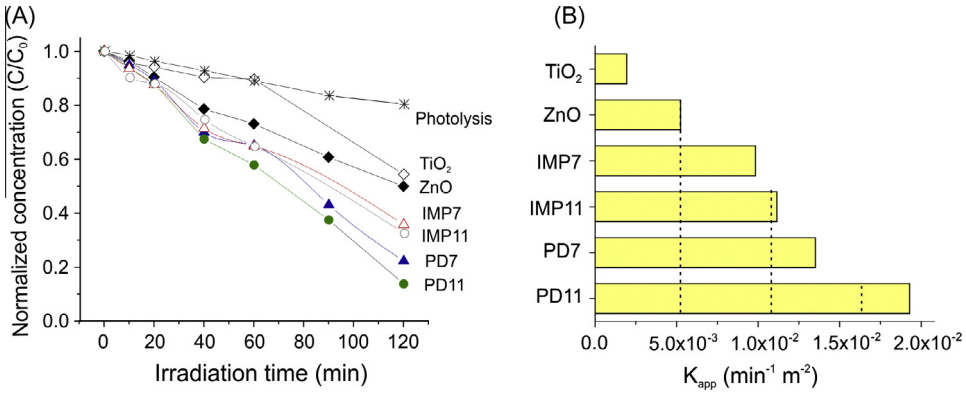

Fig. 6. Photocatalytic activity of Ag/ZnO and surface area normalized rate constant of bisphenol-A degradation.

face area. The apparent rate constants of pure ZnO and P25 TiO_2 was were found to be very close (0.00578 and 0.00484 min^{-1}, respectively). However, after normalization, the K_{app} of pure ZnO was three times the value of TiO_2 P25 because of the differences in specific surface area (Table 3). Surface-area normalized rate constants of Ag/ZnO photocatalysts were higher for photodeposited samples than for impregnated ones. The 1% w/w Ag/ZnO-PD11,1 was the most active photocatalyst, with a normalized K_{app} equal to 0.01929 min^{-1} m^{-2}, 3.7 times the value for pure ZnO (Fig. 6B). The decreasing order of degradation rates was Ag/ZnO-PD > Ag/ZnO-IMP > ZnO > P25.

The improvement in the photocatalytic performance of Ag/ZnO was attributed to the silver nanoparticles, which act to trap the photoexcited electron in the metallic bond [12,13]. In this way, higher primary (e^{*-}–h^+ pair) and secondary (free radicals, i.e., ·OH) active species remain longer on the photocatalyst surface to improve the photocatalytic activity through oxidation of bisphenol-A.

These results show that the photocatalytic performance was not related to the specific surface area but to the catalytic sites, the chemical composition of the surface, and ionized surface groups induced by pH.

4. Conclusions

We report two functionalization methods, photodeposition and impregnation, which promote homogeneous distribution of AgNPs on ZnO. Nevertheless, the two methods follow different mechanisms of interaction; in the case of the photodeposited photocatalyst, the UV irradiation ensures a stronger interaction between Ag and ZnO. In this work we used the actual amount of silver attached to the ZnO surface, as the response of the experimental design analyzed by response surface methodology. This new approach enables the optimization of the reaction conditions for the functionalization of ZnO with stabilized AgNPs through the methods reported. The attachment of AgNPs to ZnO was mainly affected by the nominal amount of AgNPs and the pH.

The photodeposited 1% w/w Ag/ZnO photocatalysts showed an increase in the lattice parameters and a decrease in BET surface area due to the insertion of Ag ions into the crystalline structure and AgNPs between ZnO pores. The small size of AgNPs and their homogeneous distribution on ZnO were observed by TEM images for both functionalization methods. In addition, hydroxyl groups on the surface and the increased visible light absorption, due to the attached AgNPs, improved the photocatalytic activity.

The resulting photodeposited 1% w/w Ag/ZnO photocatalyst showed four times higher reaction rates for the bisphenol-A degradation, compared to ZnO without silver nanoparticles. Finally, the proposed functionalization methods in this study represent a useful approach to synthesizing photocatalysts, with potential applications in environmental remediation of water contaminated with endocrine disrupting compounds.

Acknowledgments

The authors would like to thank the National Science and Technology Council of Mexico for the Ph.D. fellowship to ABJS (CONACYT-211830) and Gladys Labrada, Nicolás Cayetano, Beatriz Rivera, and Carmen Rocha for technical support. We acknowledge the use of facilities of the national laboratories LINAN and LANBAMA at the IPICYT. Authors The authors also thank Jennifer Eckerly for their suggestions to improve this manuscript.

Appendix A. Supplementary material

Supplementary data associated with this article can be found, in the online version, at http://dx.doi.org/10.1016/j.jcat.2014.06.008.

References

[1] C.A.K. Gouvêa, F. Wypych, S.G. Moraes, N. Durán, P. Peralta-Zamora, Chemosphere 40 (2000) 427–432.
[2] S. Kaneco, H. Katsumata, T. Suzuki, K. Funasaka, K. Ohta, BCSI 6 (2007) 22–33.
[3] S. Suwanboon, P. Amornpitoksuk, P. Bangrak, A. Sukolrat, N. Muensit, J. Ceram. Process Res. 11 (2010) 547–551.
[4] R. Dastjerdi, M. Montazer, Colloids Surf. B Biointerfaces 79 (2010) 5–18.
[5] A.J. Gimenez, J.M. Yañez-Limón, J.M. Seminario, J. Phys. Chem. C 115 (2011) 282–287.
[6] Z.L. Wang, X.Y. Kong, Y. Ding, P. Gao, W.L. Hughes, R. Yang, Y. Zhang, Adv. Funct. Mater. 14 (2004) 943–956.
[7] B. Li, H. Cao, J. Mater. Chem. 21 (2011) 3346–3349.
[8] Z. Xiong, L.L. Zhang, J. Ma, X.S. Zhao, Chem. Commun. 46 (2010) 6099–6101.
[9] K.M. Reddy, K. Feris, J. Bell, D.G. Wingett, C. Hanley, A. Punnoose, Appl. Phys. Lett. 90 (2007) 213902-1–213902-3.
[10] S.P. Wang, S.L. Zhong, H.L. Xu, J. Phys: Conf. Ser. 188 (2009) 012034.
[11] N. Kislov, J. Lahari, H. Verma, D.Y. Goswami, E. Stefanakos, M. Batzill, Langmuir 25 (2009) 3310–3315.
[12] R. Georgekutty, M.K. Seery, S.C. Pillai, J. Phys. Chem. C 112 (2008) 13563–13570.
[13] Y. Zheng, L. Zheng, Y. Zhan, X. Lin, Q. Zheng, K. Wei, Inorg. Chem. 46 (2007) 6980–6986.
[14] K.B. Narayanan, N. Santhivel, Adv. Colloid Interface Sci. 156 (2010) 1–13.
[15] L. Zhang, J.C. Yu, H.Y. Yip, Q. Li, K.W. Kwong, A.W. Xu, P. Wong, Langmuir 19 (2003) 10372–10380.
[16] R. Zanella, S. Giorgio, C.R. Henry, C. Louis, J. Phys. Chem. B 103 (2002) 7634–7642.
[17] M.R. Kim, S.H. Choi, J. Nanomater. (2009) 1–7.
[18] M. Demirel, K. Berkant, Int. J. Ind. Chem. 3 (2012) 3–24.
[19] R. Amadelli, L. Samiolo, A. Maldotti, A. Molinari, M. Valigi, D. Gazzoli, Int. J. Photoenergy (2008) 1–10.
[20] F. Peng, H. Zhu, H. Wang, H. Yu, Korean J. Chem. Eng. 24 (2007) 1022–1026.
[21] R. Song, Y. Liu, L. He, Solid State Sci. 10 (2008) 1563–1567.

[22] C. Chung, M. Lee, Bull. Korean Chem. Soc. 25 (2004) 1461–1462.
[23] V. Salgueiriño-Maceira, M.A. Correa-Duarte, M. Farle, A. López-Quintela, K. Sieradzki, R. Diaz, Chem. Mater. 18 (2006) 2701–2706.
[24] A. Salaün, J.A. Hamilton, D. Iacopino, S.B. Newcomb, M.G. Nolan, S.C. Padmanabhan, I.M. Povey, M. Salaün, M.E. Pemble, Thin Solid Films 518 (2010) 6921–6926.
[25] S. Gao, X. Jia, S. Yang, Z. Li, K. Jiang, J. Solid State Chem. 184 (2011) 764–769.
[26] W. Xie, Y. Li, W. Sun, J. Huang, H. Xie, X. Zhao, J. Photochem. Photobiol. A – Chem. 216 (2010) 149–155.
[27] J. Wang, X.M. Fan, K. Tian, Z.W. Zhou, Y. Wang, Appl. Surf. Sci. 257 (2011) 7763–7770.
[28] Y. Zheng, C. Chen, Y. Zhan, X. Lin, Q. Zheng, K. Wei, J. Zhu, J. Phys. Chem. C 112 (2008) 10773–10777.
[29] C. Goebbert, H. Bisht, N. Al-Dahoudi, R. Nonninger, M.A. Aegerter, H. Schmidt, J. Sol–Gel Sci. Technol. 19 (2000) 201–204.
[30] D. Chu, Y. Masuda, T. Ohji, K. Kato, Langmuir 26 (2010) 2811–2815.
[31] B.D. Ahn, H.S. Kang, J.H. Kim, G.H. Kim, H.W. Chang, S.Y. Lee, J. Appl. Phys. 100 (2006) 093701-1–093701-6.
[32] Y.J. Kwon, K.H. Kim, C.S. Lim, K.B. Shim, J. Ceram. Process Res. 3 (2002) 146–149.
[33] S. Sakthivel, M.V. Shankar, M. Palanichamy, B. Arabindoo, D.W. Bahnemann, V. Murugesan, Water Res. 38 (13) (2004) 3001–3008.
[34] K. Shimizu, H. Kawachi, S. Komai, K. Yoshida, Y. Sasaki, A. Satsuma, Catal. Today 175 (2011) 93–99.
[35] B. Mukherjee, B. Viswanath, N. Ravishankar, J. Phys. D Appl. Phys. 43 (2010) 455301.
[36] D. Zhou, A.A. Keller, Water Res. 44 (2010) 2948–2956.
[37] N.V. Kaneva, C.D. Dushkin, Colloids Surf. A 382 (2011) 211–218.
[38] L. Zhang, L. Yin, C. Wang, N. Lun, Y. Qi, ACS Appl. Mater. Interfaces 6 (2) (2010) 1769–1773.
[39] A.V. Emeline, V.N. Kuznetsov, V.K. Ryabchuk, N. Serpone, Environ. Sci. Pollut. Res. 19 (2012) 3666–3675.
[40] N. Clament Sagaya Selvam, J. Judith Vijaya, L. John Kennedy, J. Colloid Interface Sci. 407 (2013) 215–224.
[41] A. Patil, K. Patil, S. Pardeshi, J. Solid State Chem. 184 (2011) 3273–3279.